Supplementary Information (SI) for Materials Horizons.
This journal is © The Royal Society of Chemistry 2026

Supporting Information

Design and Engineering of Biomimetic Aloe vera Sponges via Recombination of Functionalized Peel and Gel for Enhanced Wound Healing

Yingjuan Yao, [#a] Junyi Xu, [#a] Yunzhu Zhai, [a] Duxiang Feng, [a] Miaolan He, [a] Rongyan Liu, [a] Zhuangpeng Chang, [a] Rui Zhao, [*a] Yanlin Feng, [*ac] Ruigang Hou, [*ab] and Xiao Zhang [*a]

[a] *Department of Pharmacy at The Second Hospital of Shanxi Medical University, and School of Pharmacy and Shanxi Provincial Key Laboratory of Cellular Physiological at Shanxi Medical University, Taiyuan, Shanxi 030001, P.R. China*

[b] *Medicinal Basic Research innovation Center of Chronic Kidney Disease, Ministry of Education, Shanxi Medical University, Taiyuan, Shanxi 030001, P.R. China*

[c] *Department of Cardiology, the First Hospital of Shanxi Medical University, Taiyuan, 030001, China*

E-mail addresses: zhaoray@a.sxmu.edu.cn (R. Zhao); feng@sxmu.edu.cn (Y. Feng); houruigang@sxmu.edu.cn (R. Hou); xiao.zhang1@hotmail.com, zhangxiao24@a.sxmu.edu.cn (X. Zhang).

[#] *These authors contributed equally to this paper.*

1. Stability evaluation of APNs

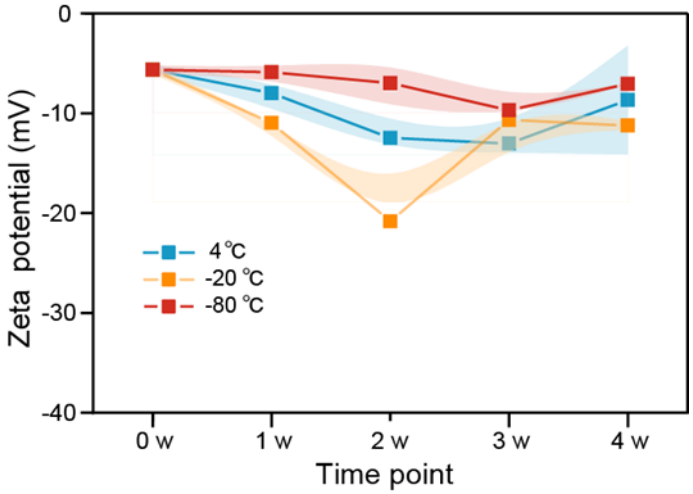

Fig. S1. Zeta potential of APNs under different storage temperatures (4, -20 and -80 ℃) for 4 weeks (n = 3).

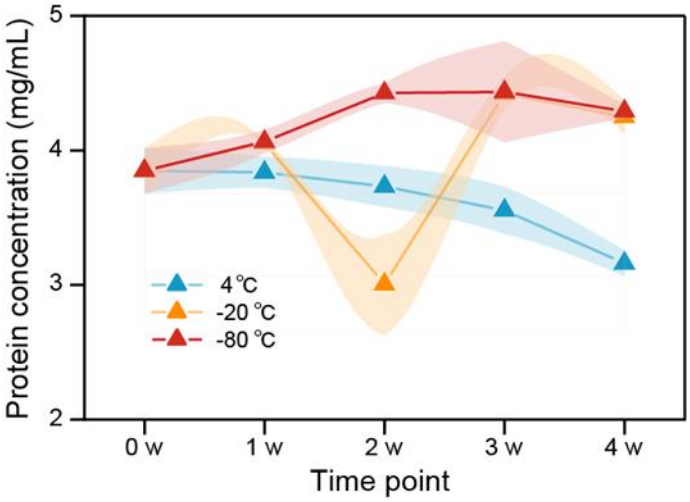

Fig. S2. Protein content of APNs under different storage temperatures (4, -20 and -80 ℃) for 4 weeks (n = 3).

2. FTIR spectrum of NEs

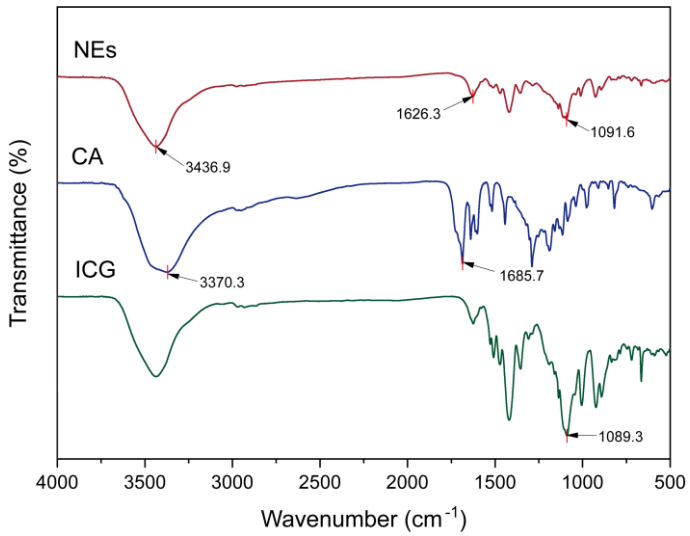

Fig. S3. FTIR spectra of CA, ICG and NEs.

3. TEM of NAPNs

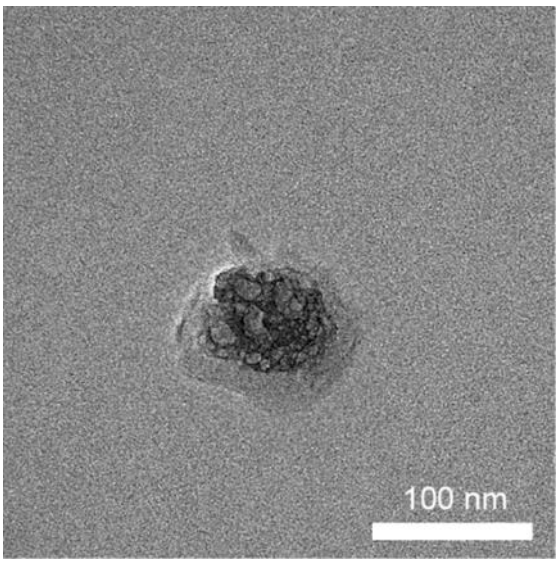

Fig. S4. The membrane structure and black contents of NAPNs. Scale bar: 100 nm.

4. Characterization of particle size and zeta potential

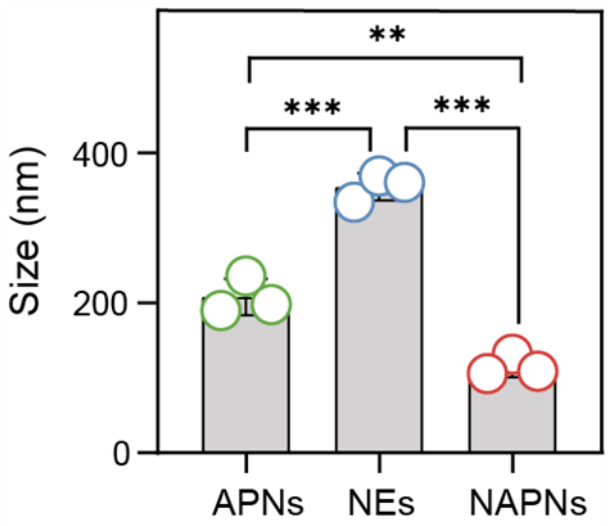

Fig. S5. Size distribution of APNs, NEs and NAPNs (n = 3). ** $p < 0.01$, *** $p < 0.001$.

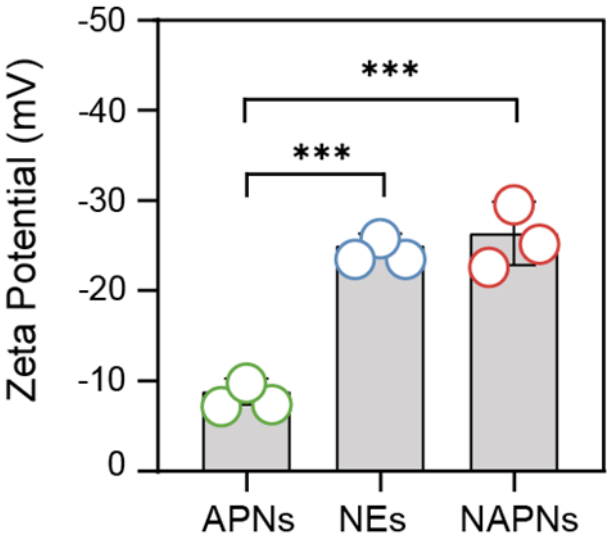

Fig. S6. Zeta Potential of APNs, NEs and NAPNs (n = 3). ***$p < 0.001$.

5. Encapsulation efficiency and drug loading of NAPNs

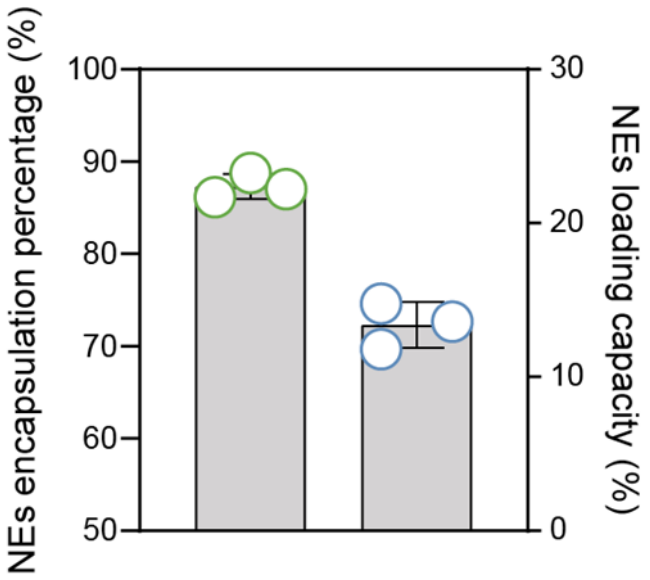

Fig. S7. Encapsulation efficiency and loading capacity of NAPNs (n = 3).

6. Temperature variations at different powers of NAPNs

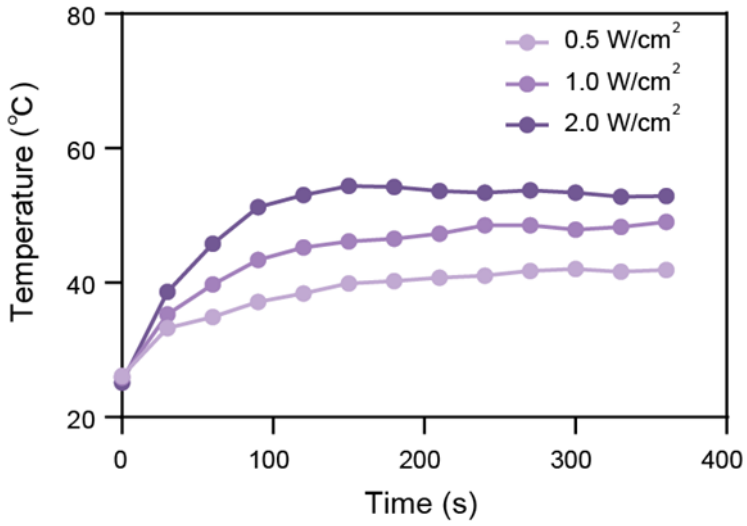

Fig. S8. Photothermal heating curves of NAPNs under different laser powers.

7. The loading efficiency

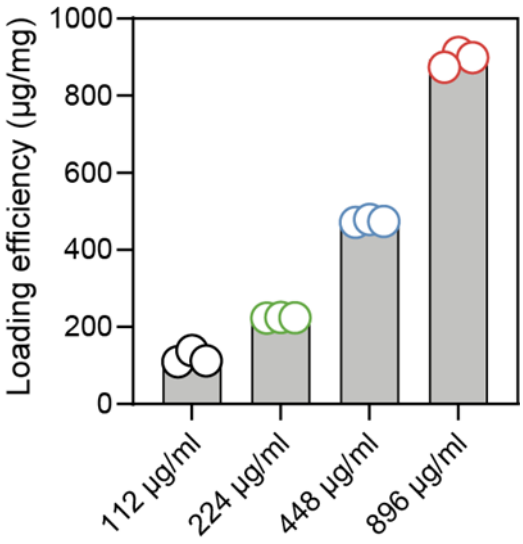

Fig. S9. The loading efficiency of AGSs for NAPNs (n = 3).

8. *In vitro* degradation

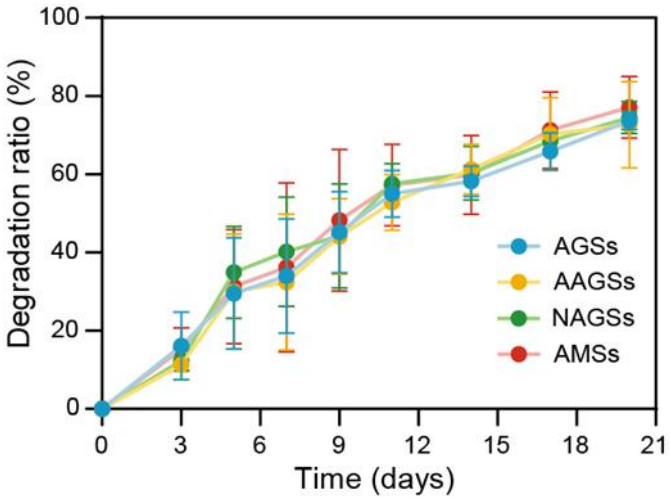

Fig. S10. *In vitro* degradation of the sponges in PBS over 21 days (n = 3).

9. Temperature changes under different power levels of AMSs

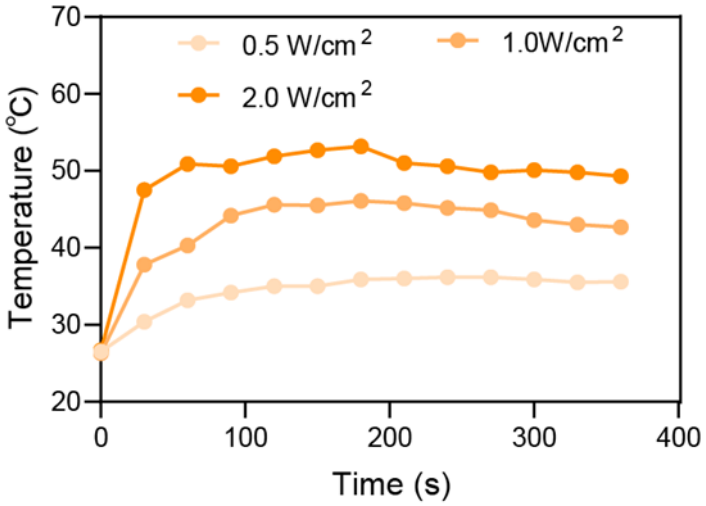

Fig. S11. Photothermal heating curves of AMSs under different laser powers.

10. Anti MRSA effects of AMSs in Vitro

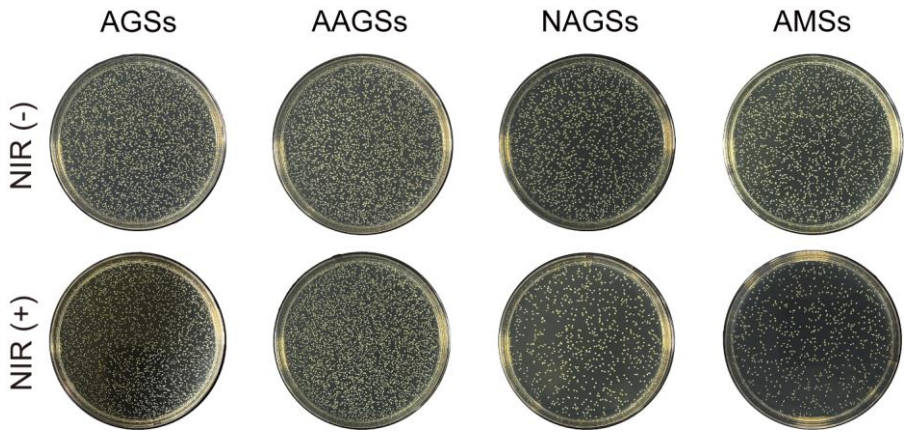

Fig. S12. Agar plate images showing MRSA growth following different treatments.

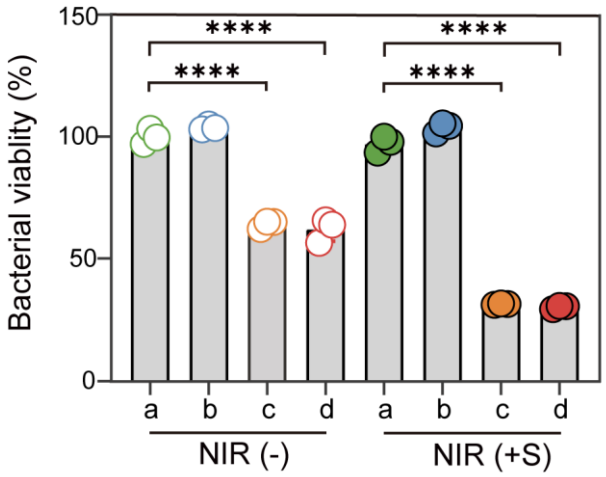

Fig. S13. Corresponding quantitative analysis of bacterial colonies. The groups are labeled as follows: a - AGSs, b - AAGSs, c - NAGSs, d - AMSs. Data were presented as mean ± s.d. ****$p < 0.0001$.

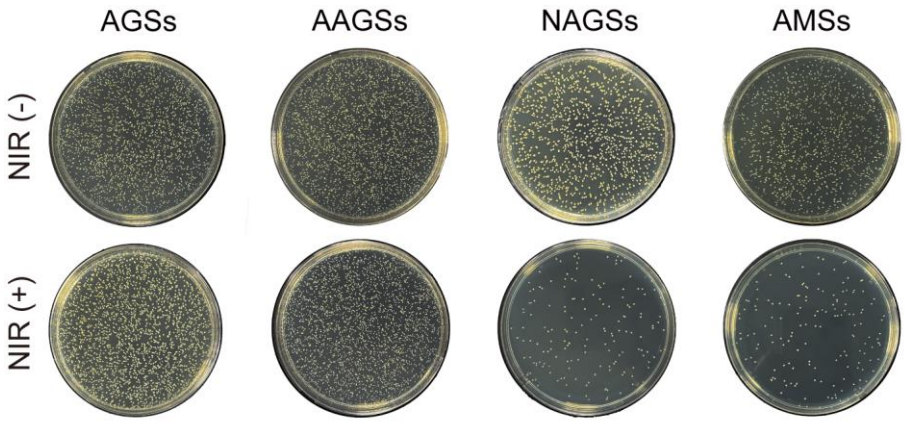

Fig. S14. Agar plate images of MRSA after treatments with NO donor addition.

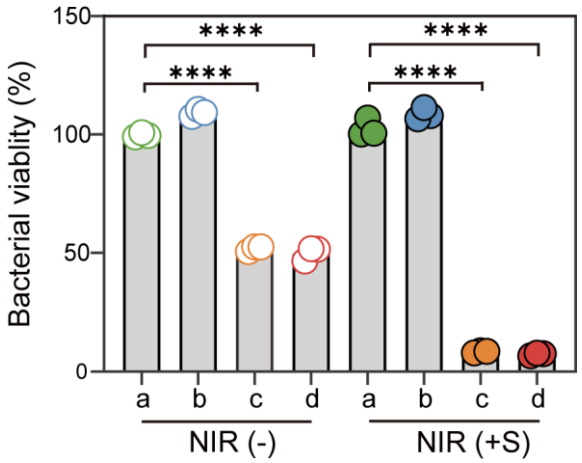

Fig. S15. Corresponding quantitative analysis of bacterial reduction (n = 3). The groups are labeled as follows: a - AGSs, b - AAGSs, c - NAGSs, d - AMSs. Data were presented as mean ± s.d. ****$p < 0.0001$.

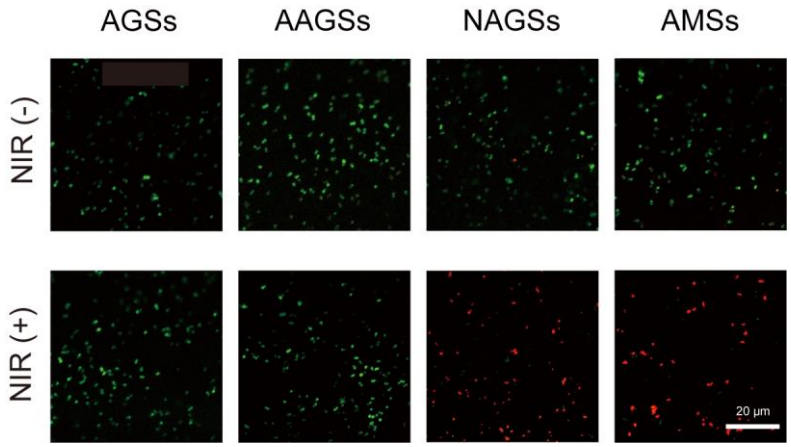

Fig. S16. Confocal fluorescence images of MRSA stained with Calcein-AM/PI under different treatment conditions. Scale bar: 20 μm.

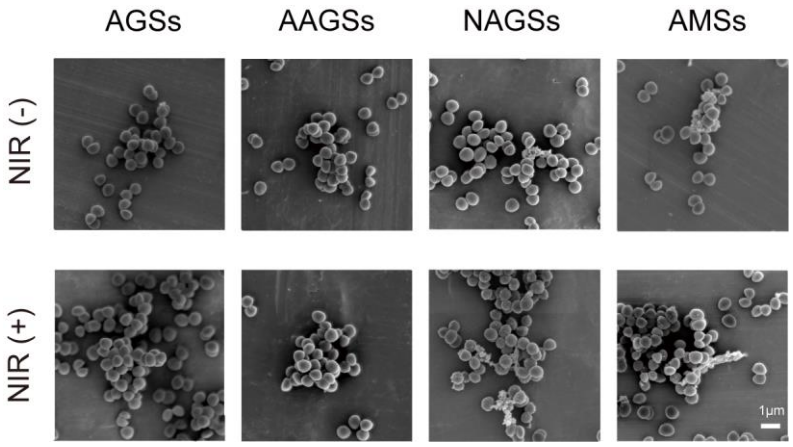

Fig. S17. SEM images of MRSA treated with various sponges, before and after laser irradiation. Scale bar: 1 μm.

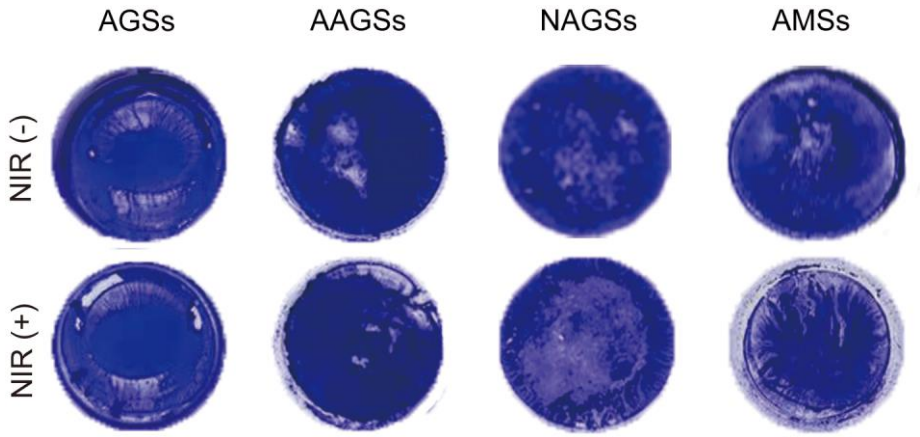

Fig. S18. Crystal violet-stained images of MRSA biofilms after different treatments.

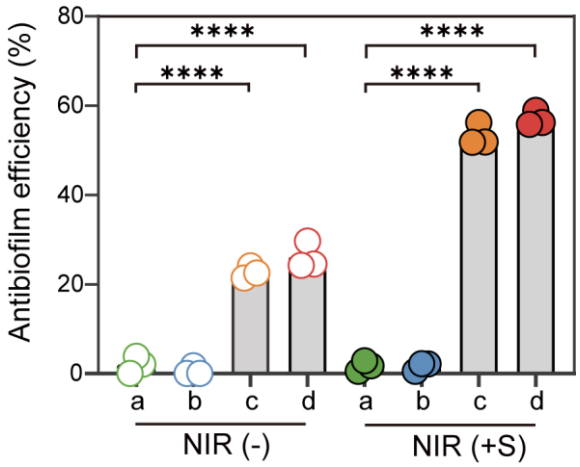

Fig. S19. Quantitative analysis of antibiofilm efficiency across treatments (n = 3). The groups are labeled as follows: a - AGSs, b - AAGSs, c - NAGSs, d - AMSs. Data were presented as mean ± s.d. ****$p < 0.0001$.

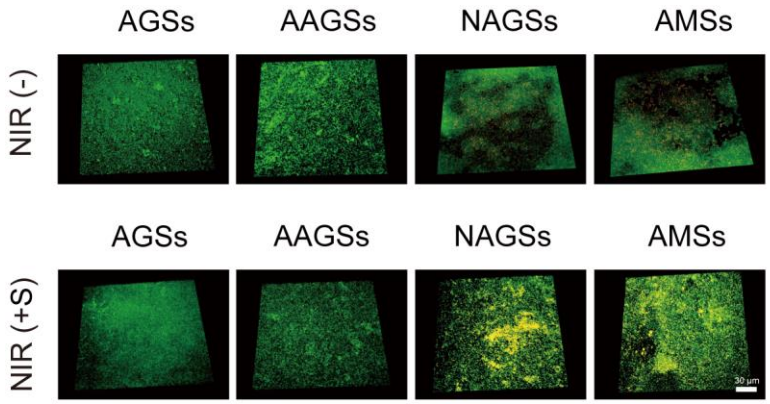

Fig. S20. 3D confocal fluorescence images of MRSA biofilm stained with Calcein-AM/PI under different treatment conditions. Scale bar: 30 μm.

11. Screening of LPS concentration

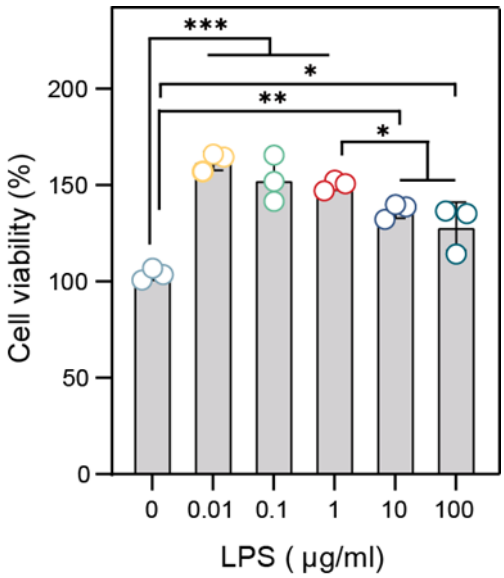

Fig. S21. The effect of LPS concentrations on RAW 264.7 (n = 3). *$p < 0.05$, **$p < 0.01$, ***$p < 0.001$.

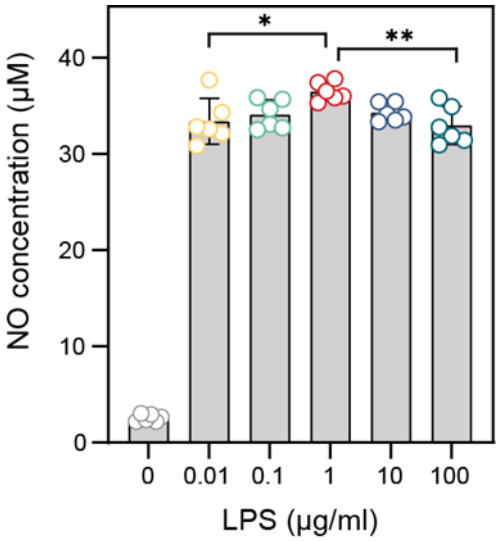

Fig. S22. NO production after stimulation with different concentrations of LPS (n = 6). *p < 0.05, **p < 0.01.

12. Quantitative analysis of TGF-β

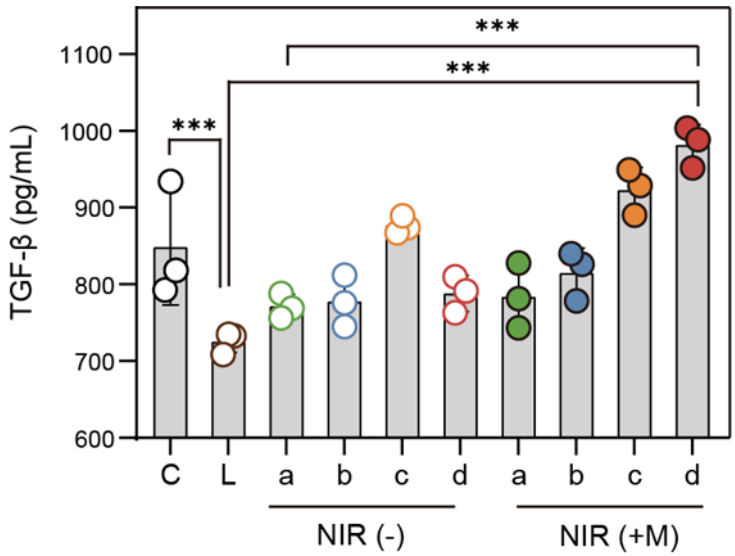

Fig. S23. Levels of TGF-β in LPS-induced RAW 264.7 cells after treatments. The letters C, L, a, b, c and d represent the control group and the experimental groups treated with LPS, AGSs, AAGSs, NAGSs and AMSs, respectively (n = 3). ***$p < 0.001$.

13. RT-qPCR analysis

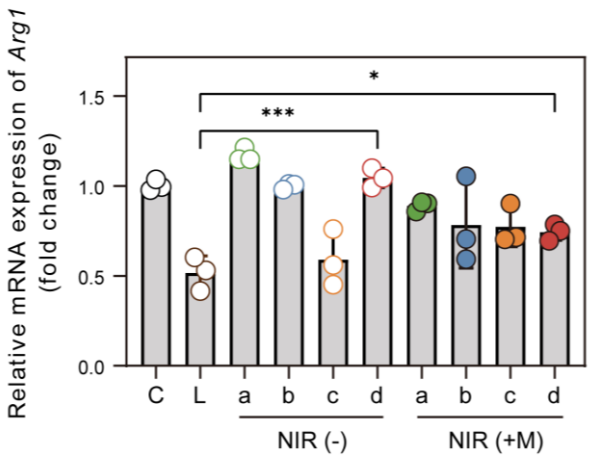

Fig. S24. The mRNA expression levels of *Arg1* in Raw 264.7 cells detected by RT-qPCR. Groups are labeled as follows: C - Control group, L - LPS only group, a - AGSs, b - AAGSs, c - NAGSs, d - AMSs. Data were presented as mean ± s.d. *$p < 0.05$, ***$p < 0.001$.

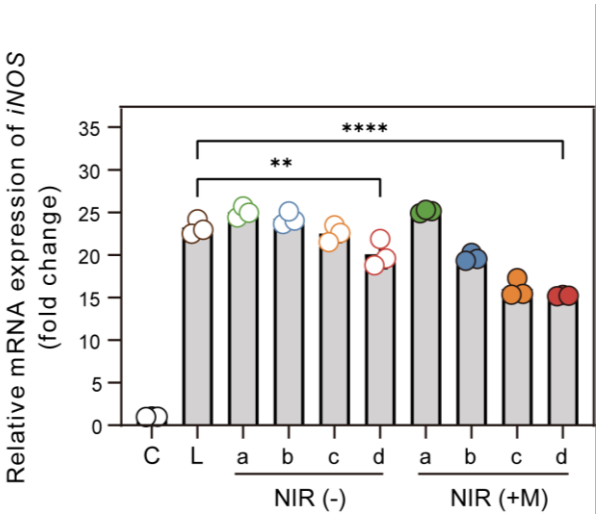

Fig. S25. The mRNA expression levels of *iNOS* in Raw 264.7 cells detected by RT-qPCR. Groups are labeled as follows: C - Control group, L - LPS only group, a - AGSs, b - AAGSs, c - NAGSs, d - AMSs. Data were presented as mean ± s.d. $^{**}p < 0.01$, $^{****}p < 0.0001$.

14. Quantitative analysis of immunofluorescence

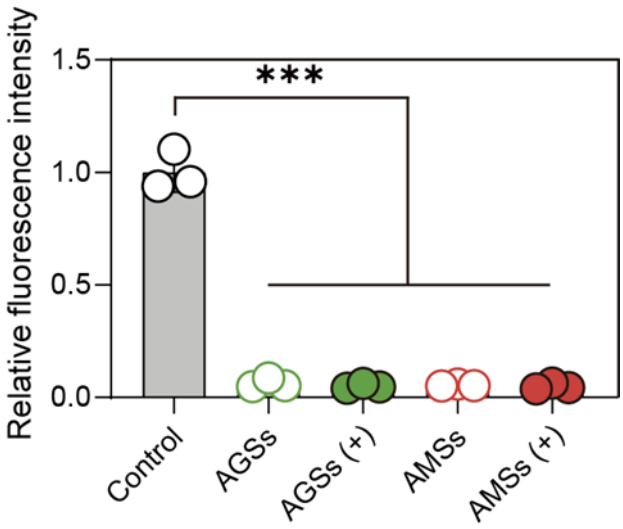

Fig. S26. Corresponding quantitative analysis of TNF-α in wound tissues (n = 3). ***$p < 0.001$.

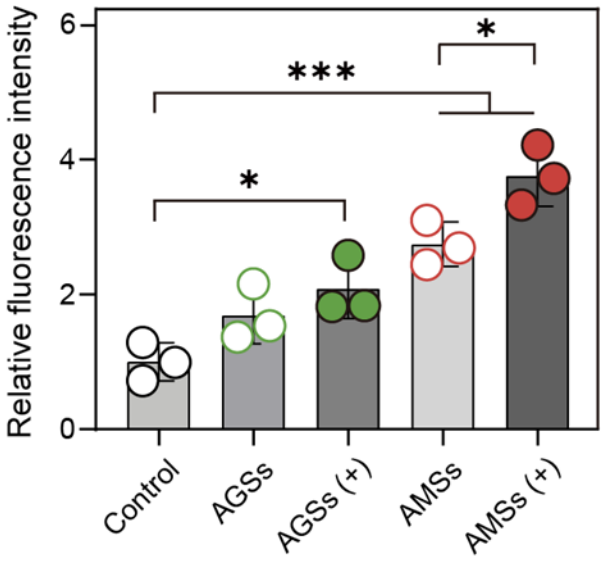

Fig. S27. Corresponding quantitative analysis of TGF-β in wound tissues (n = 3). *$p < 0.05$, ***$p < 0.001$.

15. In vivo evaluation of biosafety of different sponges

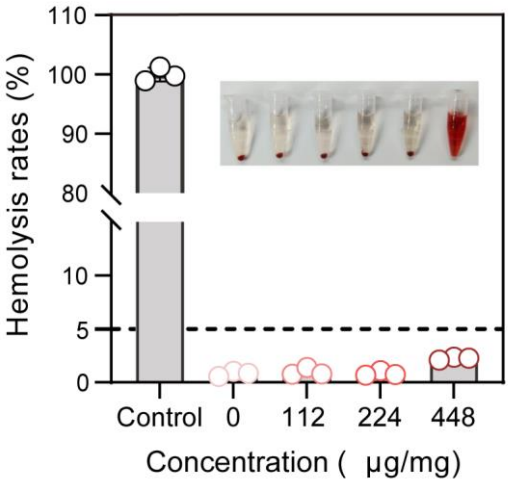

Fig. S28. *In vitro* hemolysis results of different concentration of AMSs. The inserted image shows hemolysis of PBS, 0 μg/mg of AMSs, 112 μg/mg of AMSs, 224 μg/mg of AMSs, 448 μg/mg of AMSs and Water (from left to right).

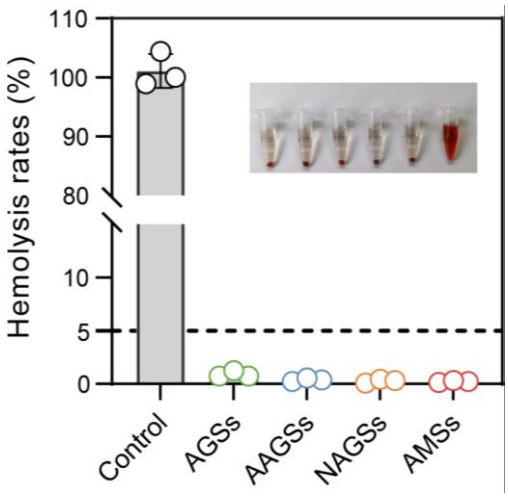

Fig. S29. *In vitro* hemolysis results of different sponges. The inserted image shows hemolysis of PBS, AGSs, AAGSs, NAGSs, AMSs and Water (from left to right).

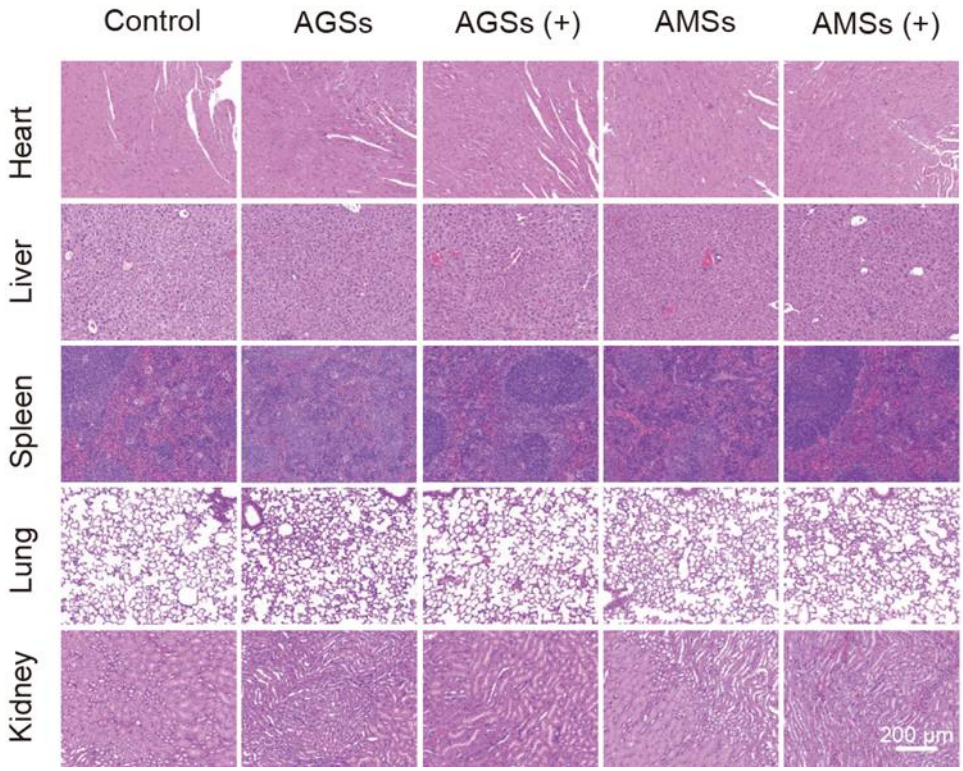

Fig. S30. H&E staining images of major organs. Scale bar: 200 μm.

16. Transcriptome sequencing results of skin wound tissues

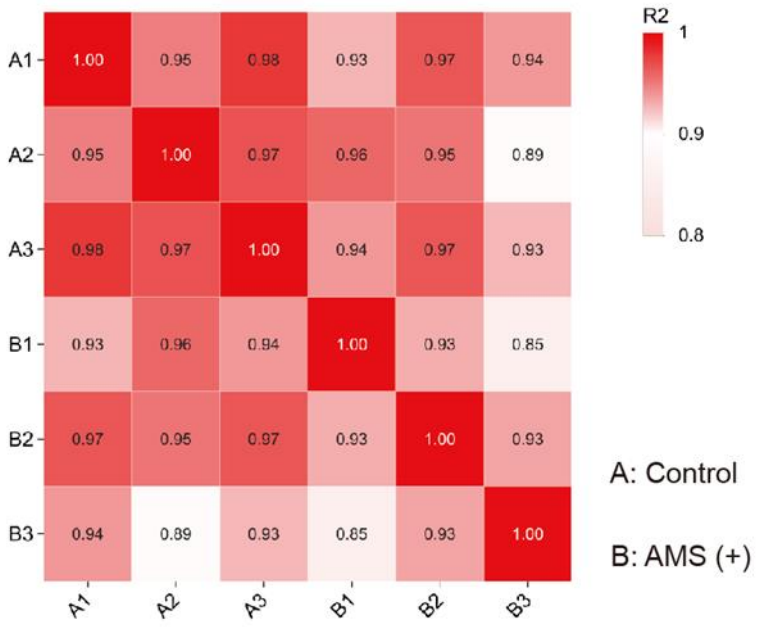

Fig. S31. The intergroup correlation of samples. Group A was the control group, Group B was the AMS (+) group.

17. GSEA analysis of gene sets

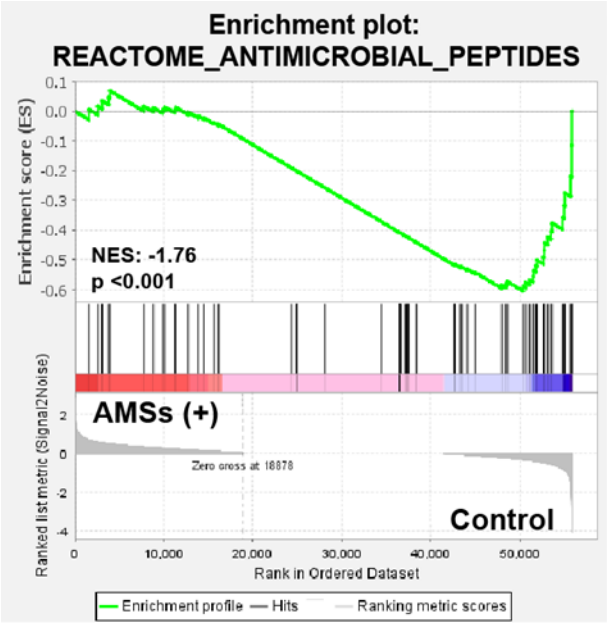

Fig. S32. GSEA analysis showing the enriched pathway: antimicrobial peptides.

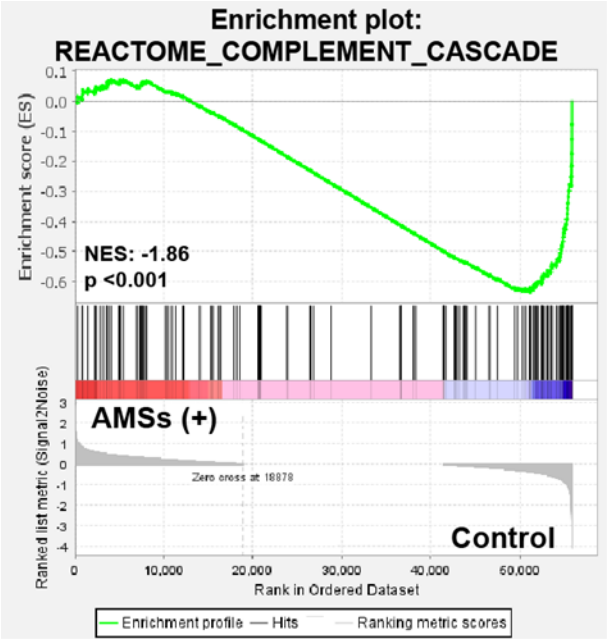

Fig. S33. GSEA analysis showing the enriched pathway: complement cascade.

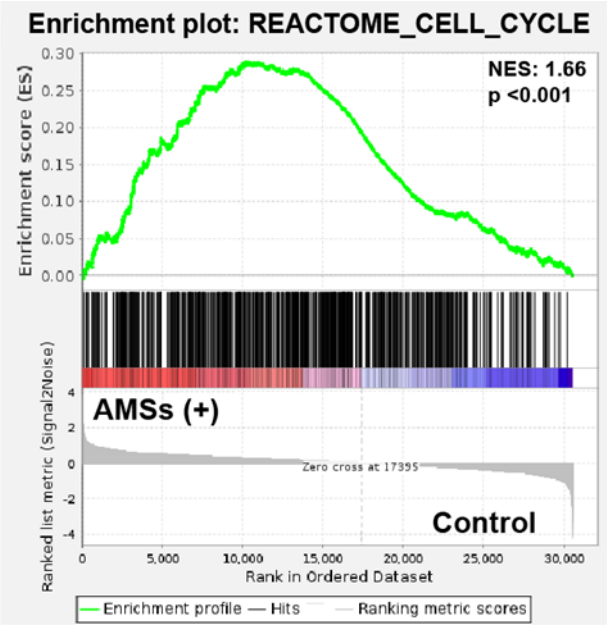

Fig. S34. GSEA analysis showing the enriched pathway: cell cycle.

18. Images and quantitative analysis of immunohistochemical staining

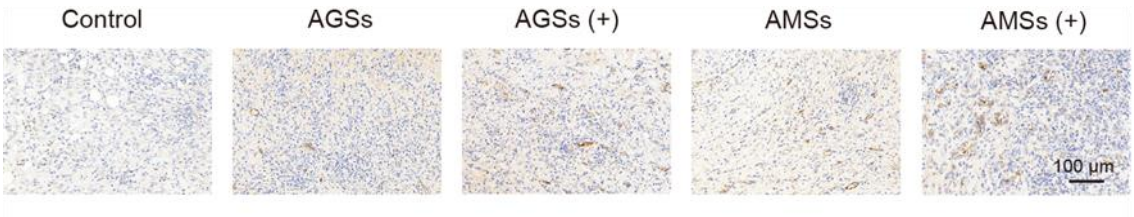

Fig. S35. Immunohistochemical diagram for FGG of infected skin wounds on day 10. Scale bar: 100 μm.

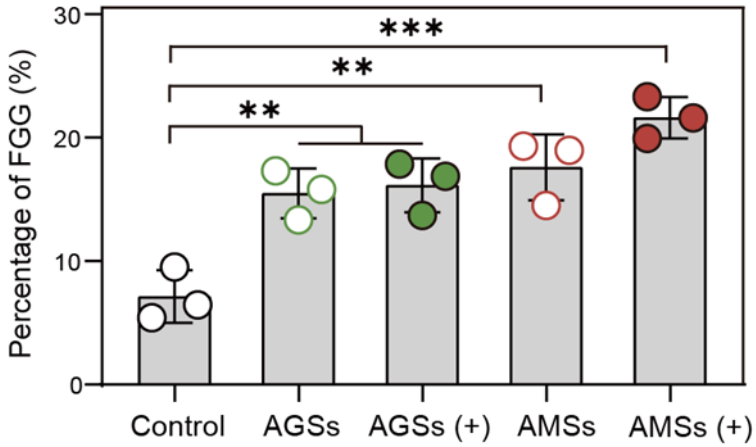

Fig. S36. Quantitative analysis of immunohistochemical staining for FGG in wound tissues (n = 3). **$p < 0.01$, ***$p < 0.001$.

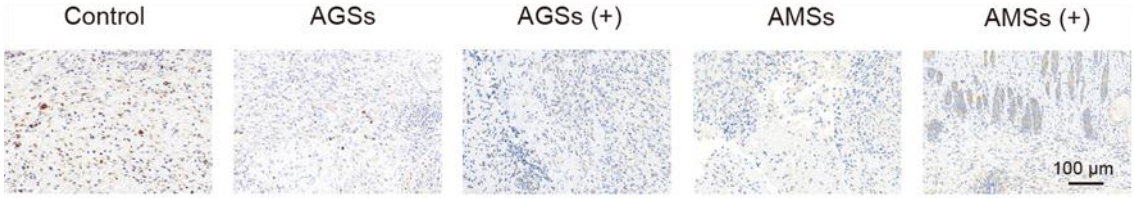

Fig. S37. Immunohistochemical diagram for CAMP of infected skin wounds on day 10. Scale bar: 100 μm.

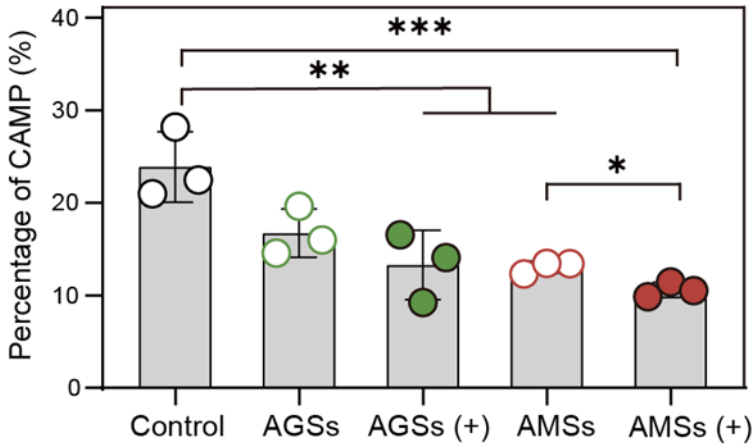

Fig. S38. Quantitative analysis of immunohistochemical staining for CAMP in wound tissues (n = 3). *$p < 0.05$, **$p < 0.01$, ***$p < 0.001$.

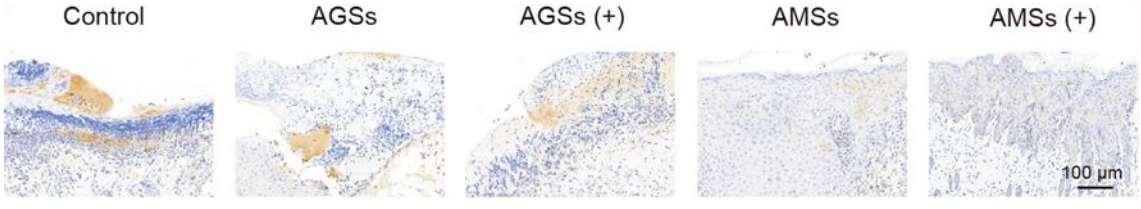

Fig. S39. Immunohistochemical diagram for CCL5 of infected skin wounds on day 10. Scale bar: 100 μm.

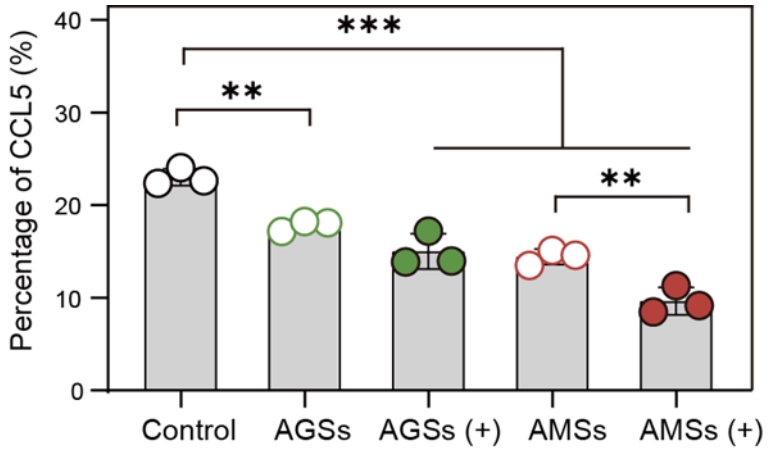

Fig. S40. Quantitative analysis of immunohistochemical staining for CCL5 in wound tissues (n = 3). $^{**}p < 0.01$, $^{***}p < 0.001$.

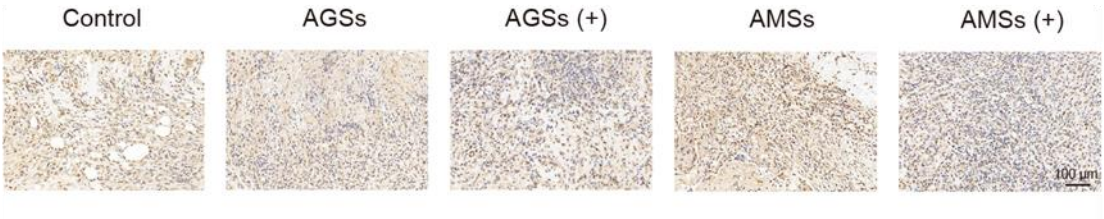

Fig. S41. Immunohistochemical diagram for TNFRSF12A of infected skin wounds on day 10. Scale bar: 100 μm.

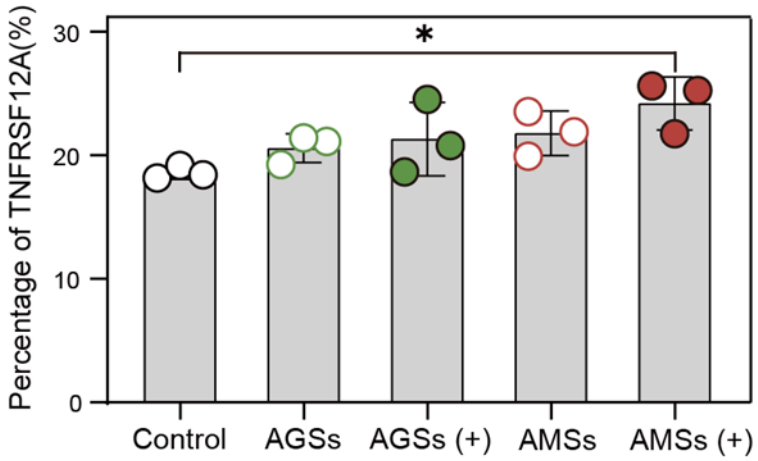

Fig. S42. Quantitative analysis of immunohistochemical staining for TNFRSF12A in wound tissues (n = 3). *$p < 0.05$.